Supporting Information for

Machine-Learning Guided Discovery of Ultralow-Threshold Organic Gain Materials Towards Electrically Pumped Lasing

Yueting Zhang[+][a], Haofeng Zheng[+][b], Zhen Dong*[a], Yanan Liu[b], Qi Liu[b], Jin Xiao[b], Yanlong Wang[b], Shuai Pang[b], Xuyu Ma[b], Qing Liao[c], Shaocong Hou*[b, d]

[a]*School of Chemistry, Chemical Engineering and Life Sciences, Wuhan University of Technology, Wuhan 430070, PR China. E-mail: bbcczhen@126.com*

[b]*School of Electrical Engineering and Automation, Wuhan University, Wuhan 430072, PR China. E-mail: sc.hou@whu.edu.cn*

[c]*Beijing Key Laboratory for Optical Materials and Photonic Devices, Capital Normal University, Beijing, 100048, PR China*

[d]*Wuhan University Shenzhen Institute, Shenzhen 518057, PR China*

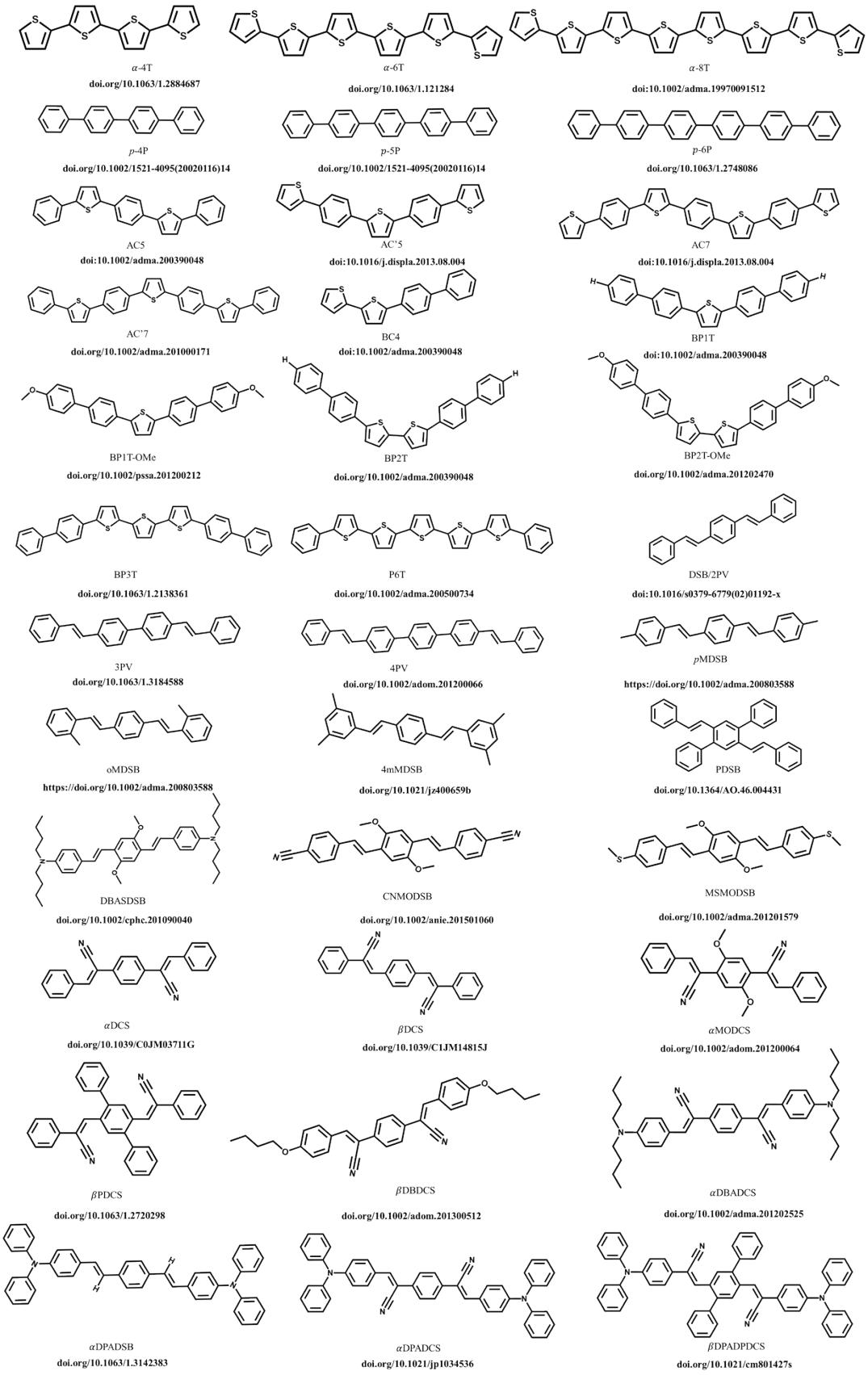

Figure S1 Organic single crystals used in the machine learning dataset

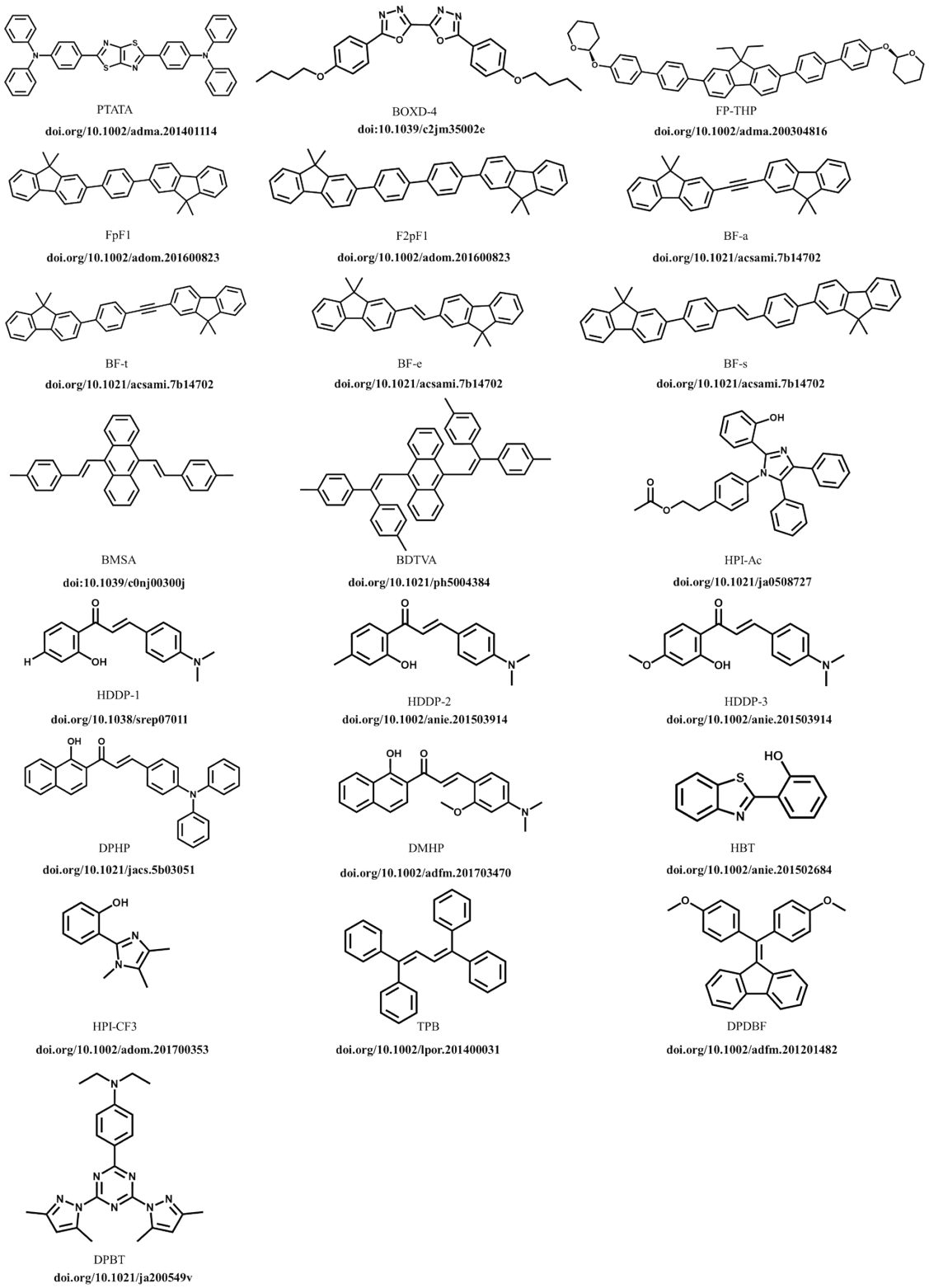

Figure S2 Organic single crystals used in the machine learning dataset

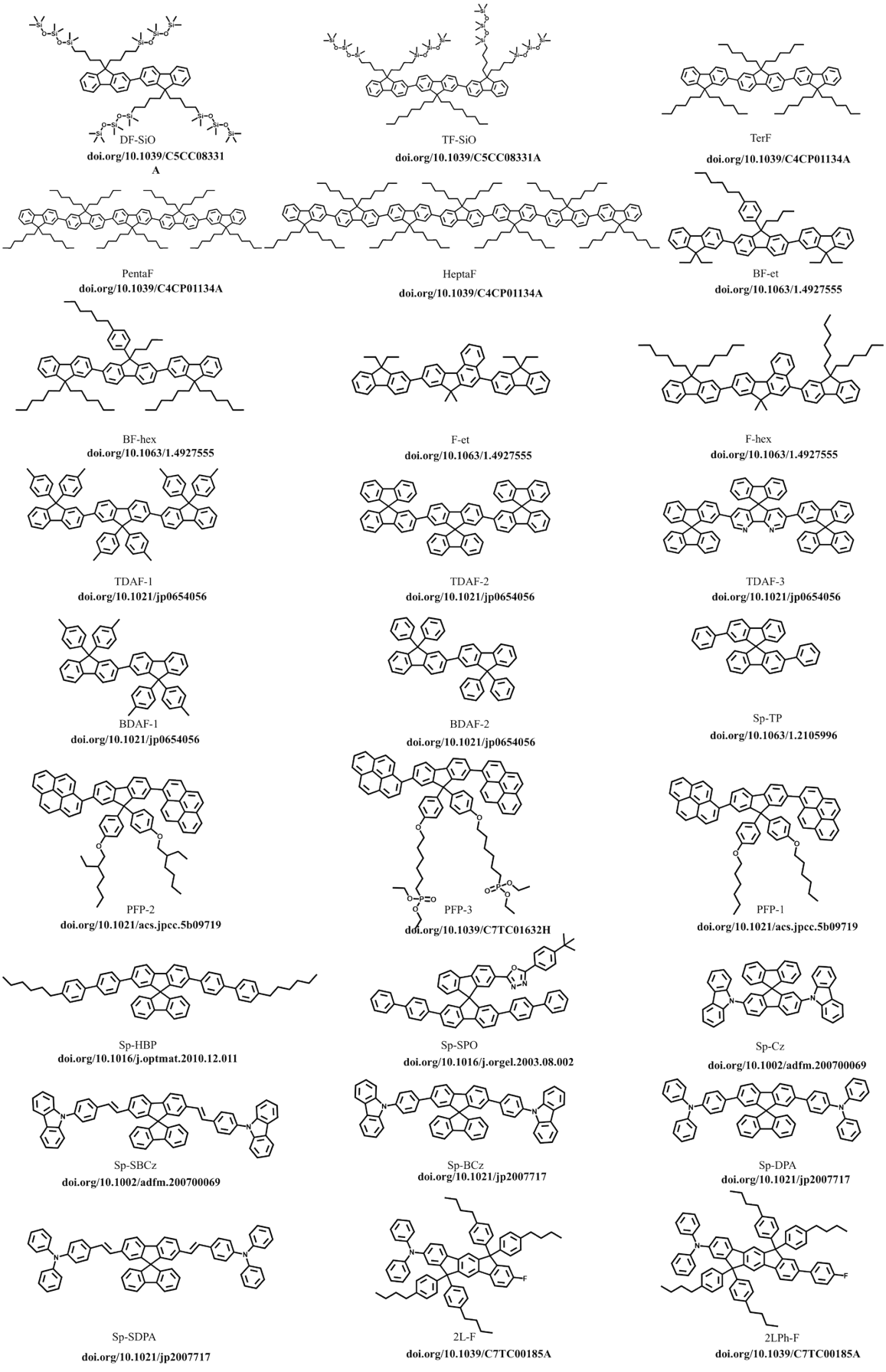

Figure S3 Small molecular gain media used in the machine learning dataset

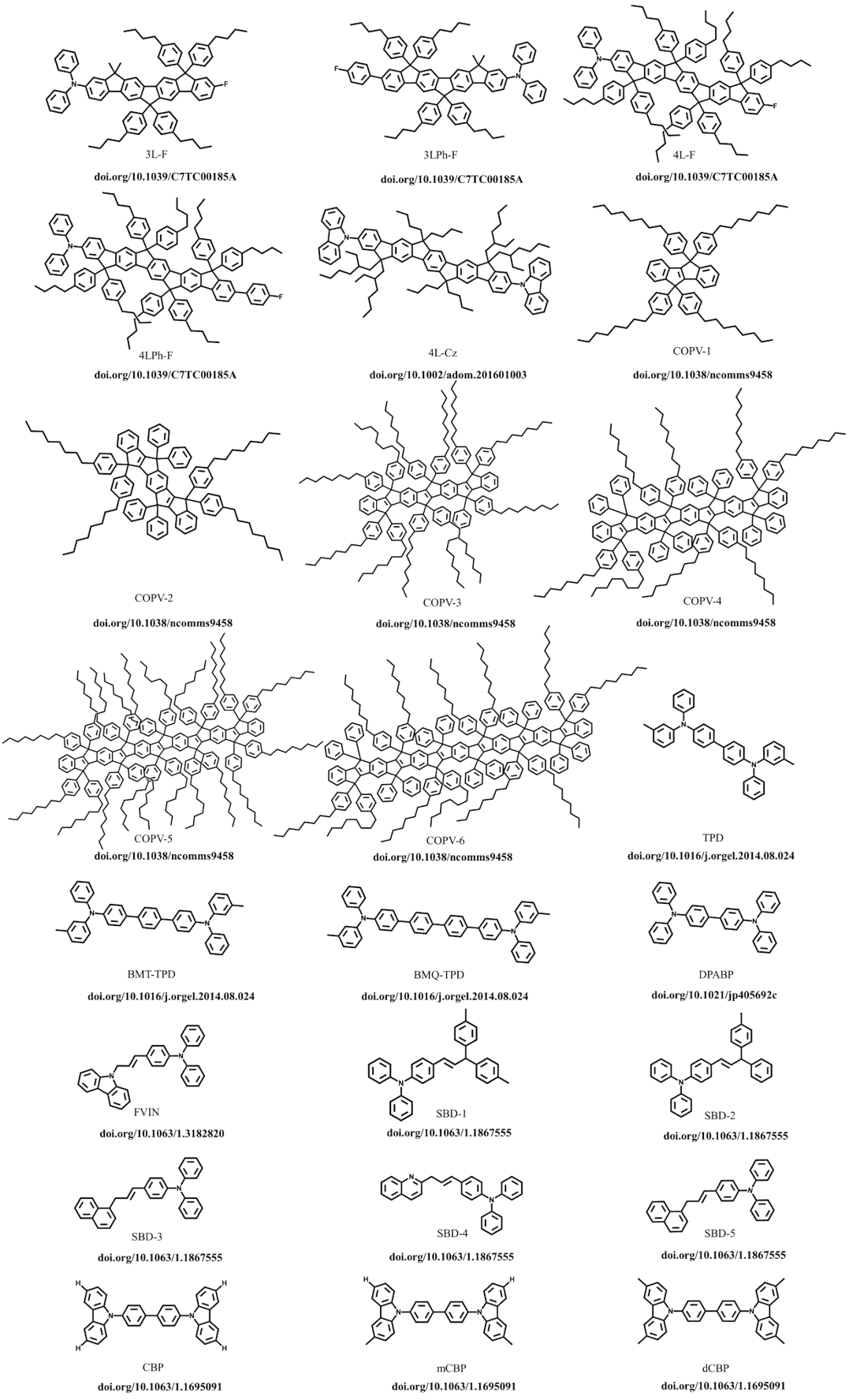

Figure S4 Small molecular gain media used in the machine learning dataset

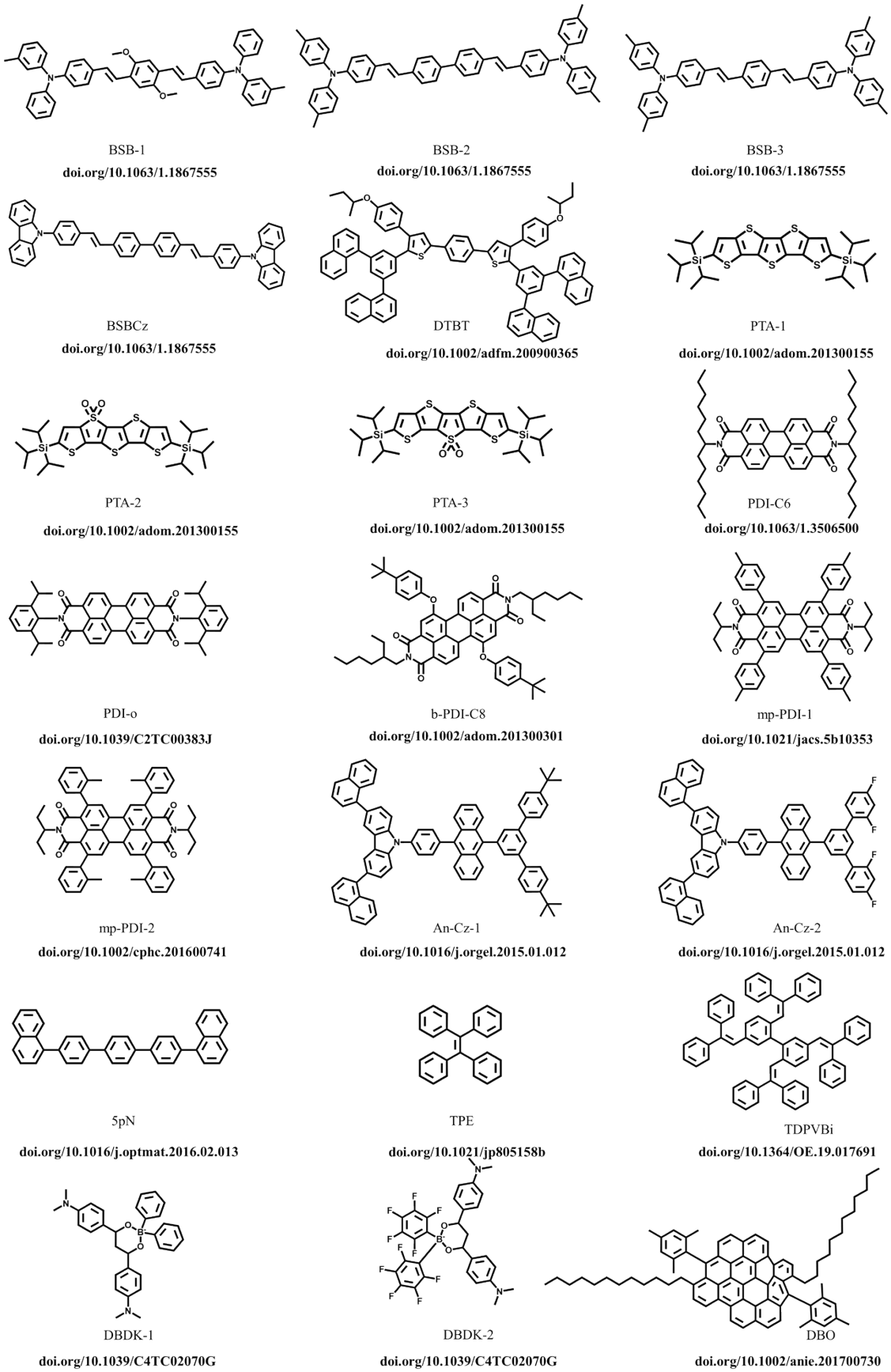

Figure S5 Small molecular gain media used in the machine learning dataset

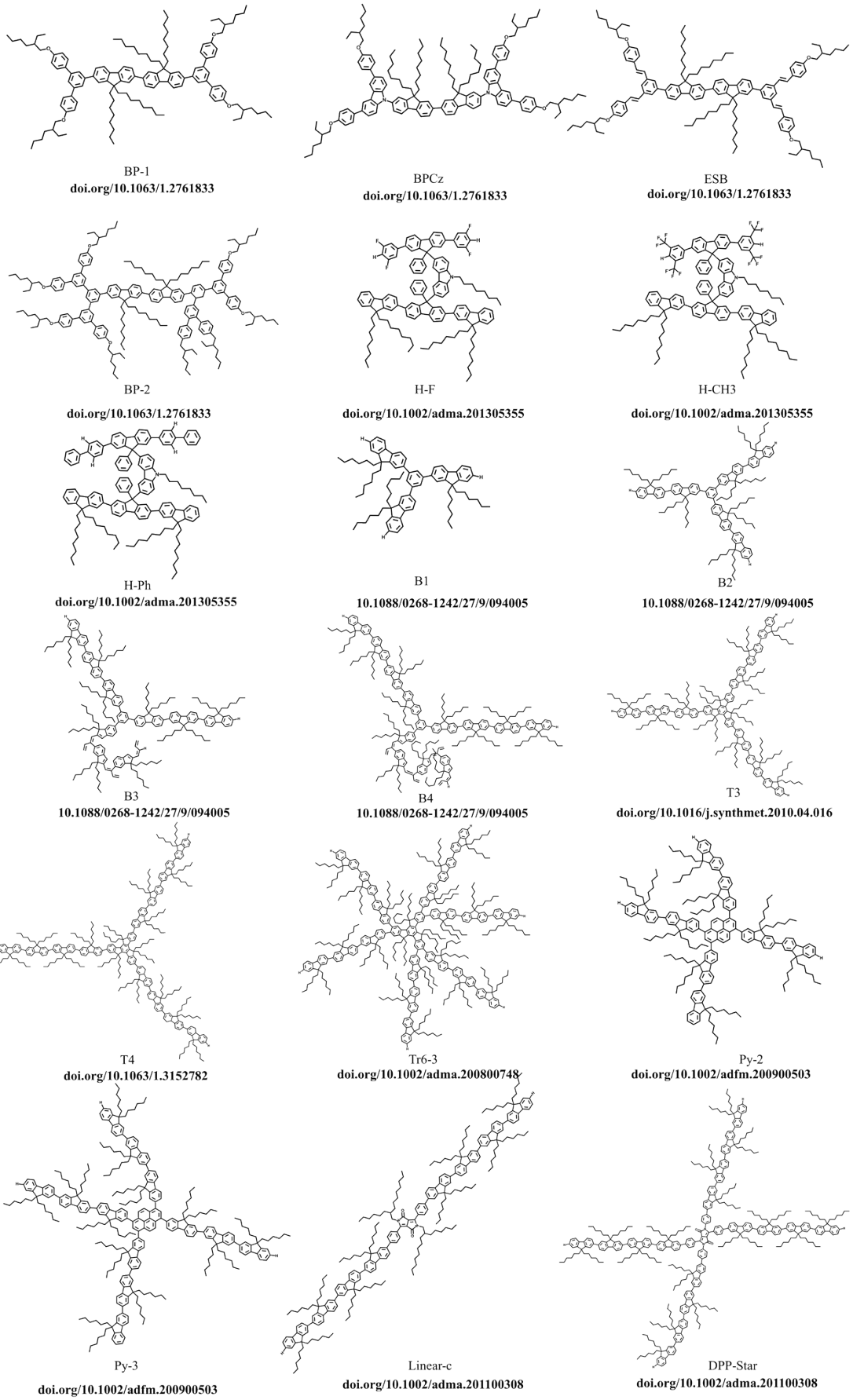

Figure S6 Dendritic starbursts used in the machine learning dataset

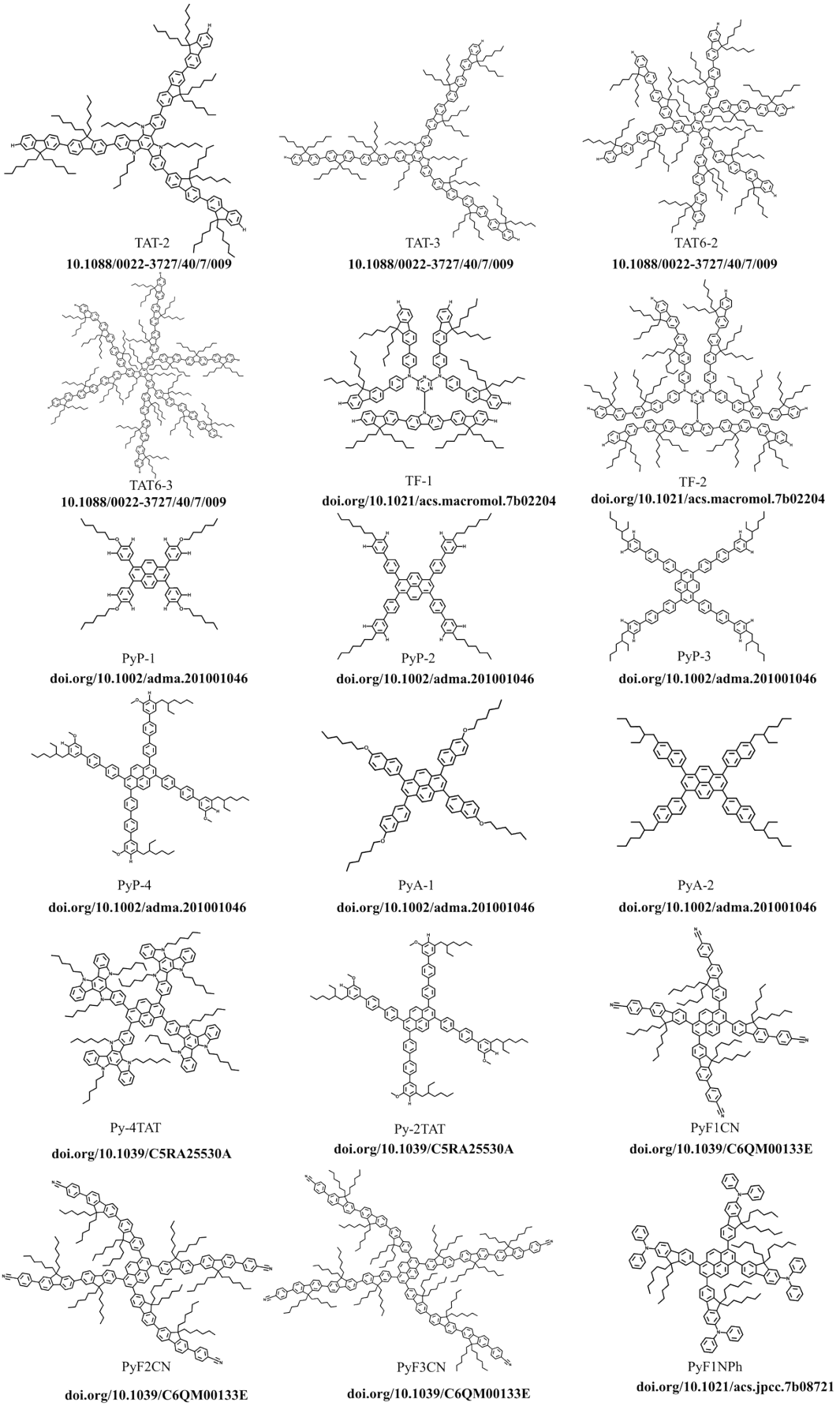

Figure S7 Dendritic starbursts used in the machine learning dataset

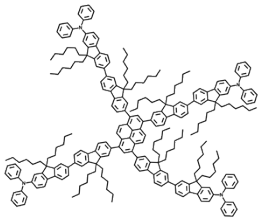

PyF2NPh

doi.org/10.1021/acs.jpcc.7b08721

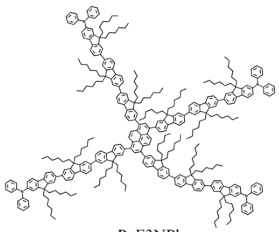

PyF3NPh

doi.org/10.1021/acs.jpcc.7b08721

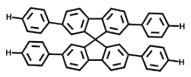

Sp-P1

doi.org/10.1002/(SICI)1521-4095(199810)10

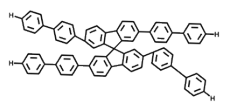

Sp-P2

doi.org/10.1002/(SICI)1521-4095(199810)10

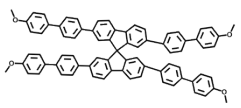

Sp-P3

doi.org/10.1016/j.orgel.2003.08.002

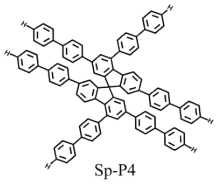

Sp-P4

doi.org/10.1016/j.orgel.2003.08.002

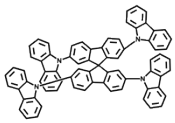

Sp-Cz

doi.org/10.1016/j.orgel.2003.08.002

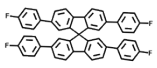

Sp-F

doi.org/10.1002/adma.200400570

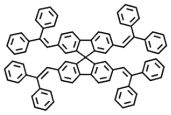

Sp-DPVBi

doi.org/10.1063/1.1792794

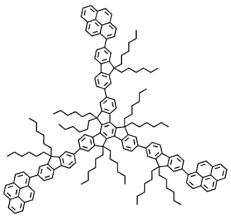

TrF1Py

doi.org/10.1002/adfm.201501337

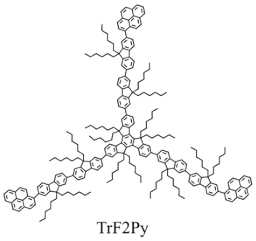

TrF2Py

doi.org/10.1002/adfm.201501337

PyFPy

doi.org/10.1039/C6TC01606E

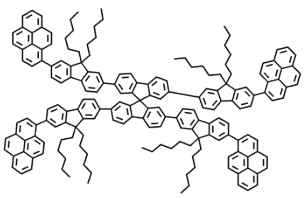

SpFPy

doi.org/10.1039/C6TC01606E

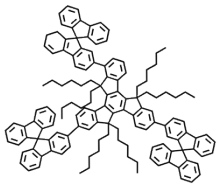

TrSp

doi.org/10.1039/C5TC01040C

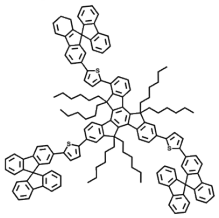

TrTSp

doi.org/10.1039/C5TC01040C

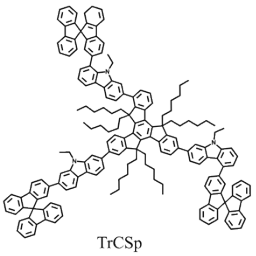

TrCSp

doi.org/10.1039/C5TC01040C

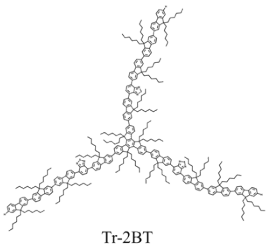

Tr-2BT

doi.org/10.1002/adfm.201202644

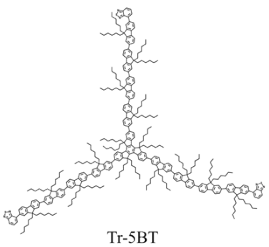

Tr-5BT

doi.org/10.1002/adfm.201202644

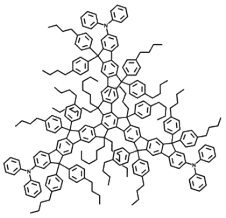

FL-1

doi.org/10.1002/chem.201605885

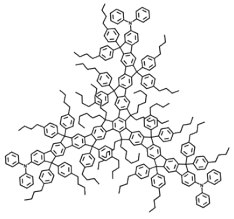

FL-2

doi.org/10.1002/chem.201605885

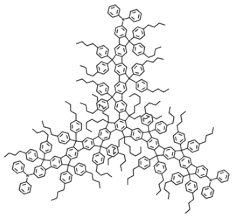

FL-3

doi.org/10.1002/chem.201605885

Figure S8 Dendritic starbursts used in the machine learning dataset

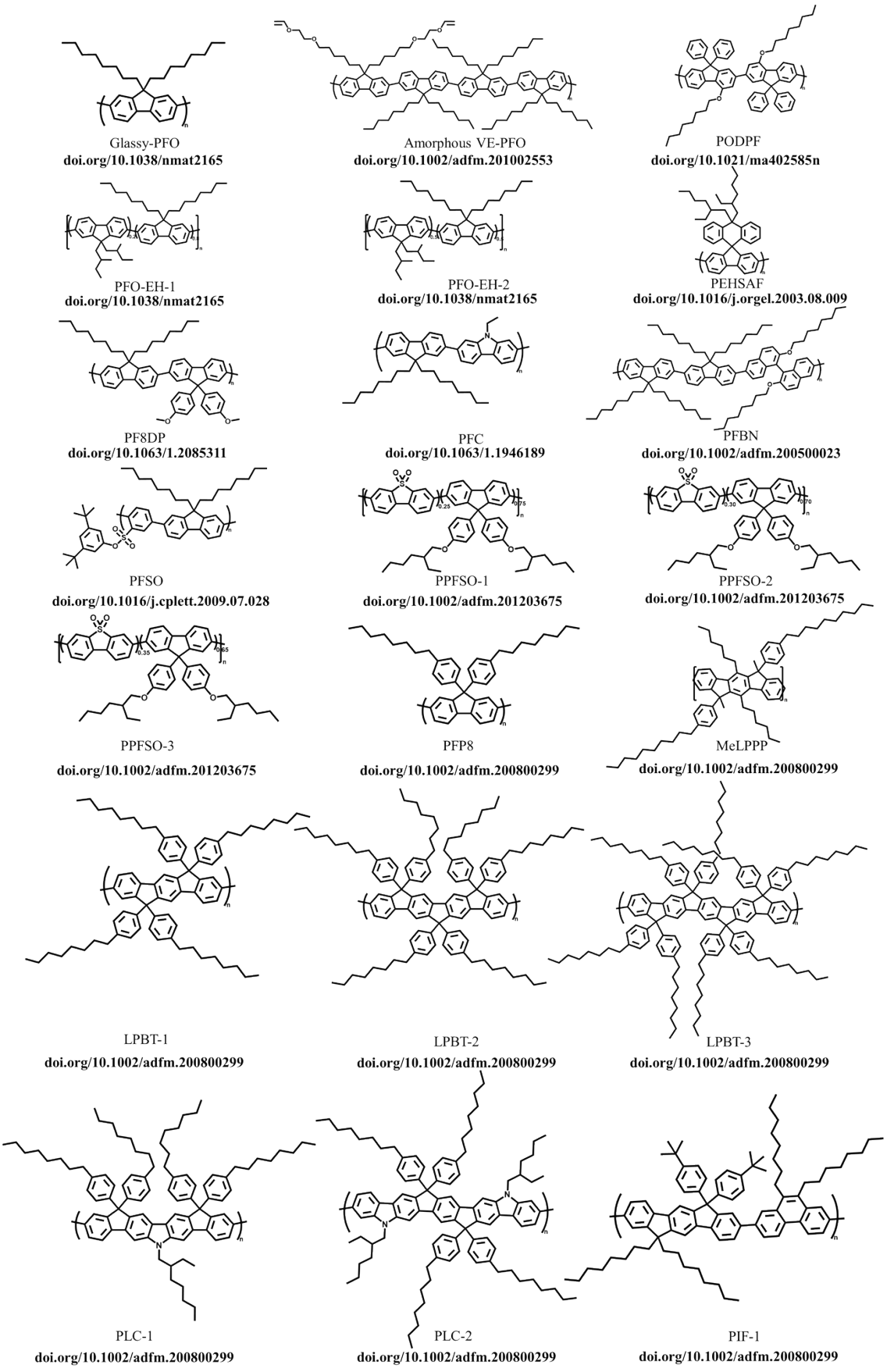

Figure S9 conjugated polymers used in the machine learning dataset

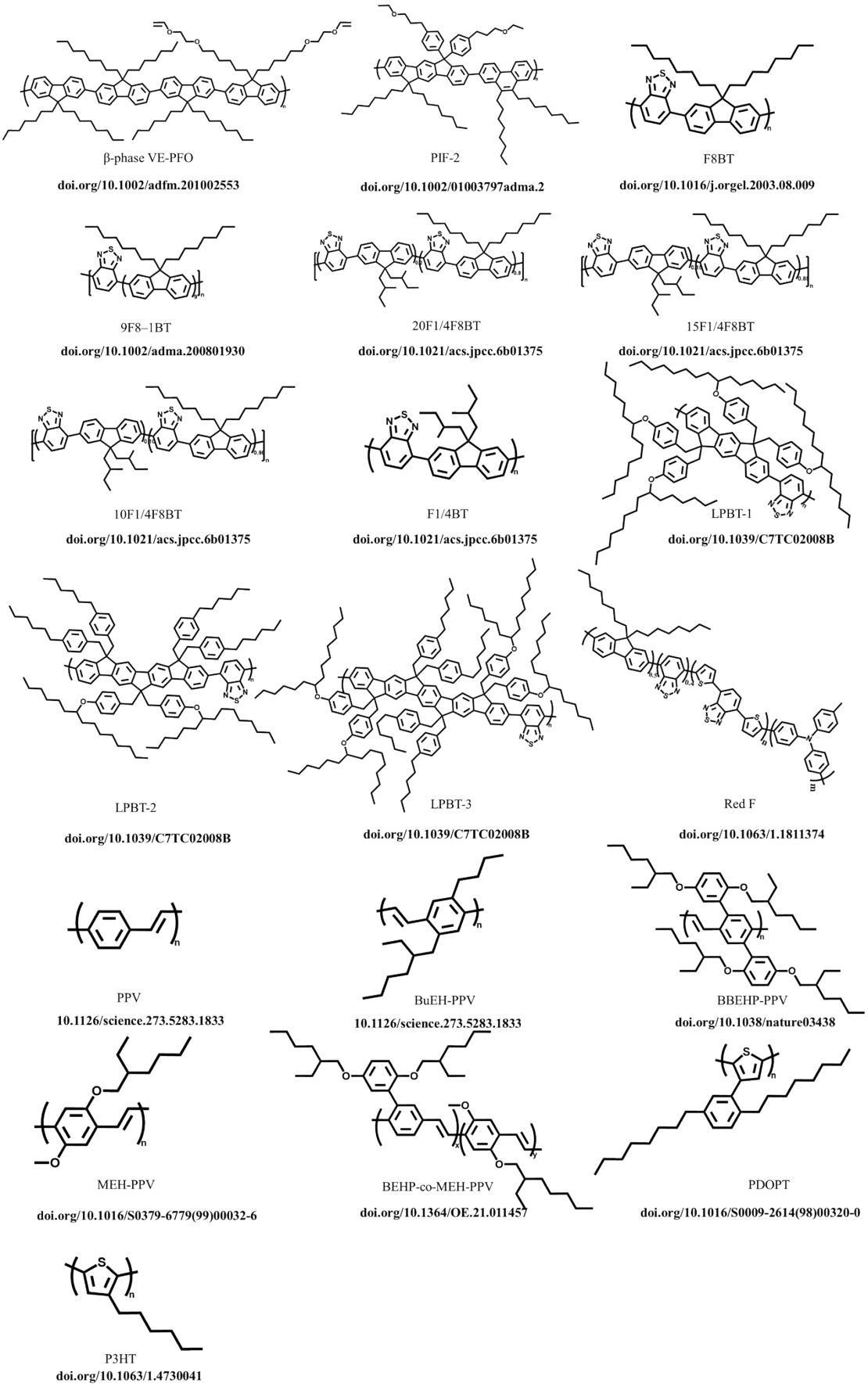

Figure S10 conjugated polymers used in the machine learning dataset

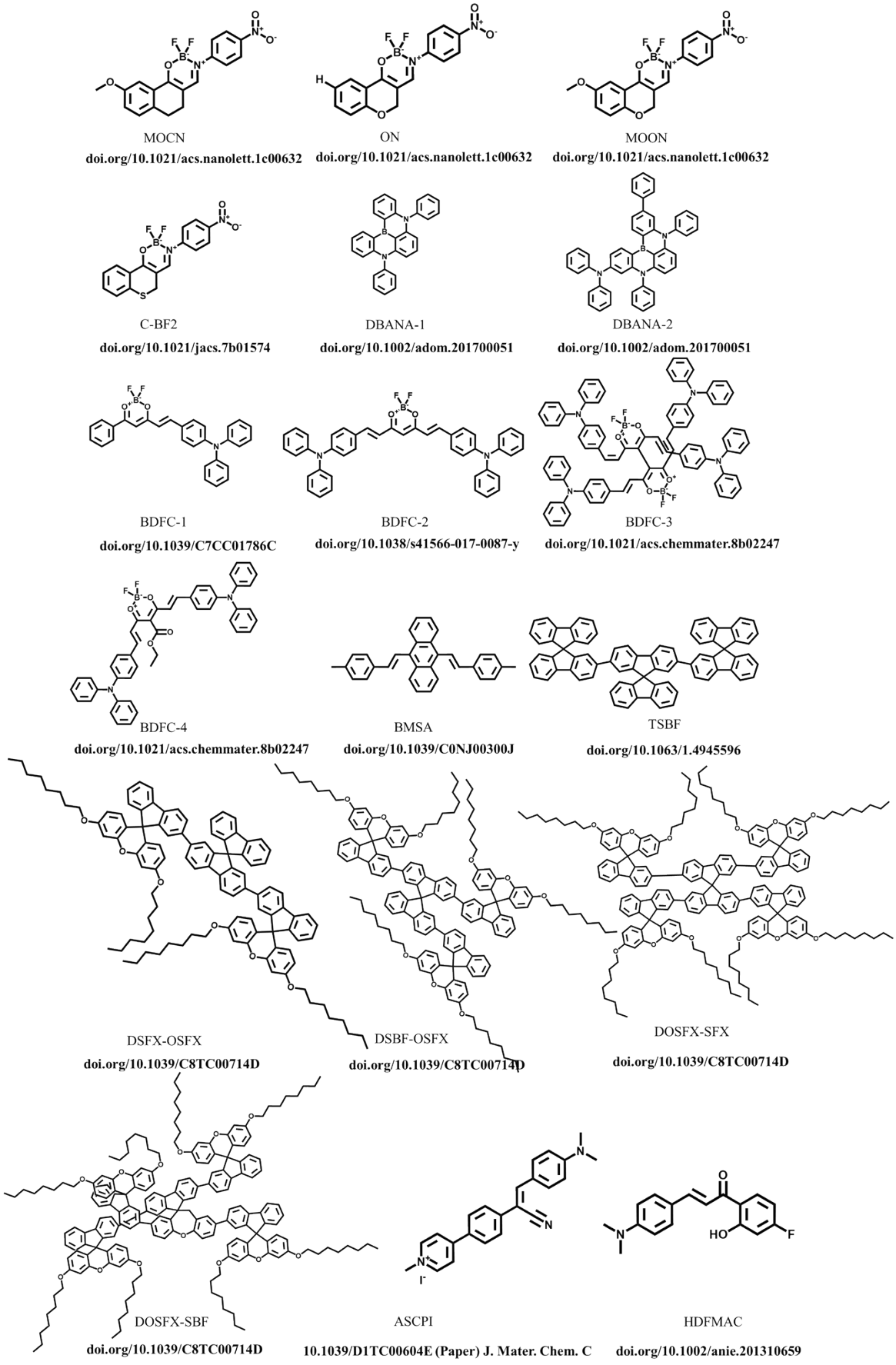

Figure S11 other molecules used in the machine learning dataset

Mathematical part

we use the root mean square error (RMSE) (eq 1) and Coefficient of determination R^2 (eq 2) to compare the performance of trained models

$$RMSE = \sqrt{\sum_{i=1}^{m} \frac{(\hat{y}_i - y_i)^2}{m}} \tag{1}$$

$$R^2 = 1 - \frac{\sum_{i=1}^{n} (\hat{y}_i - y_i)^2}{\sum_{i=1}^{n} (\bar{y}_i - y_i)^2} \tag{2}$$

where n, y_i and $\hat{y}_i$ represent the total number of data, experimental and predicted values, respectively. The $\bar{y}$ denotes the average of experimental values. The *RMSE* ranges from 0 to infinity, where smaller values indicate more accurate predictions and stronger model performance. When the R^2 values of the test and training sets are higher and converge closely, it indicates the model's robust ability to accurately explain or fit the data.

Recursive Feature Elimination (RFE)

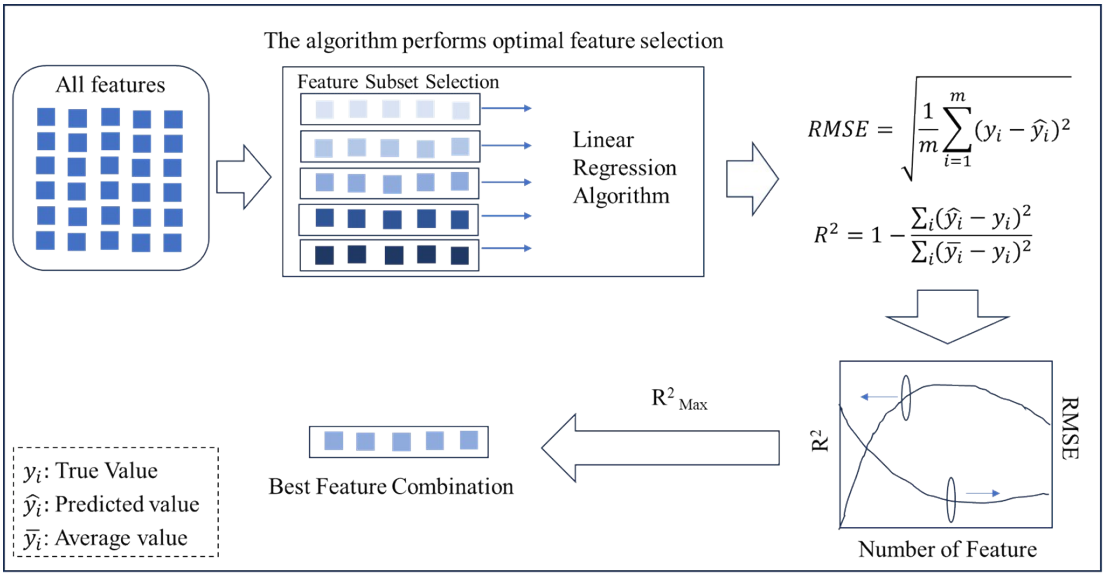

Figure S12 REF Schematic Diagram

Recursive Feature Elimination (RFE) is an algorithm that selects the optimal features by recursively removing the least important ones. The method first trains a model using all features and evaluates and ranks the importance of each feature. Then, it progressively removes the least important features, retrains the model after each elimination, and reassesses and ranks the importance of the remaining features. This process continues iteratively, comparing the model performance for each feature subset, ultimately determining the optimal feature set. RFE effectively improves the model's predictive accuracy, reduces computational complexity, and helps prevent overfitting.

Eleven trained models for the ASE threshold

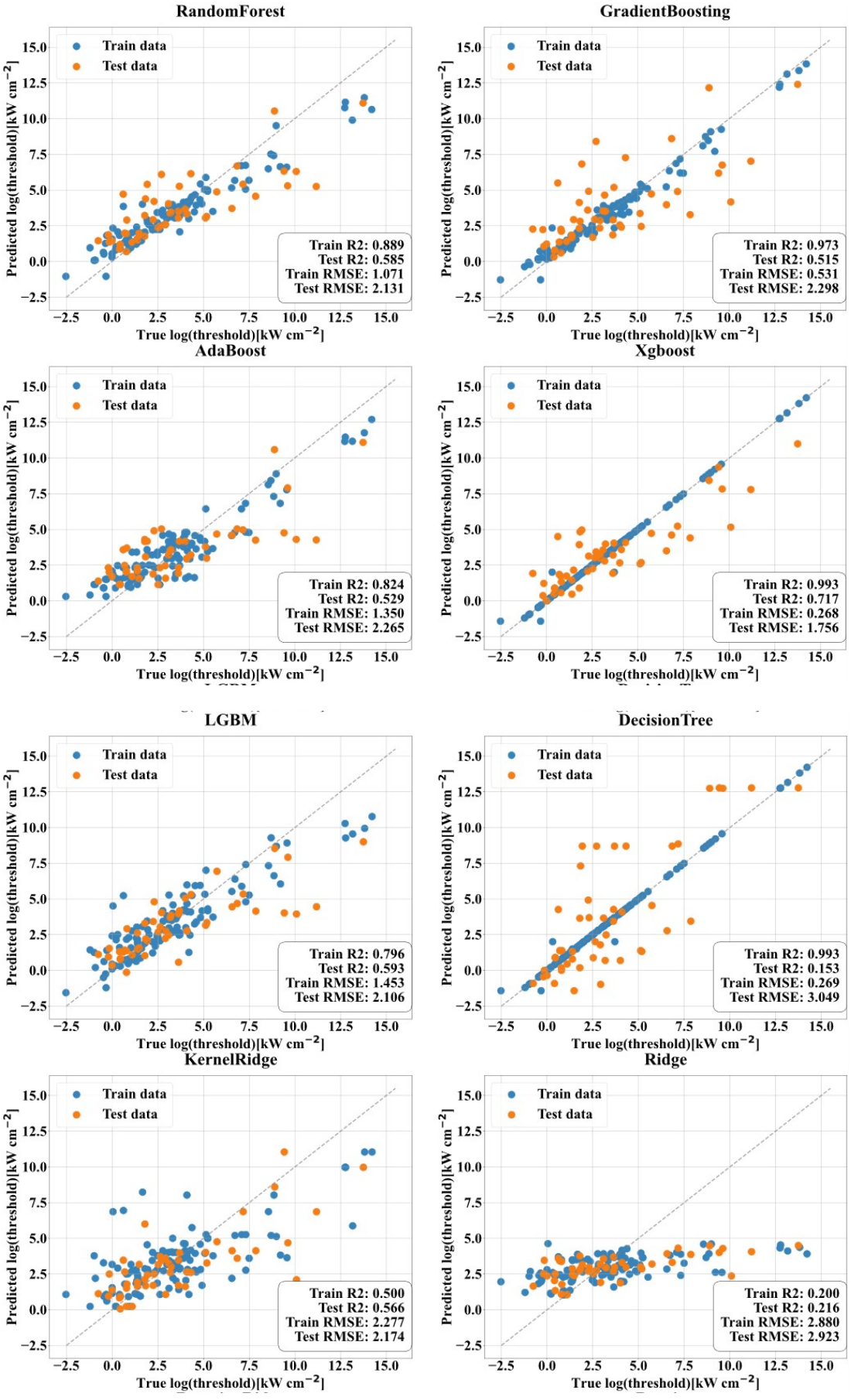

Figure S13 The fitting performance of eleven models on the training and testing sets of ASE threshold data

Eleven trained models for the ASE wavelength

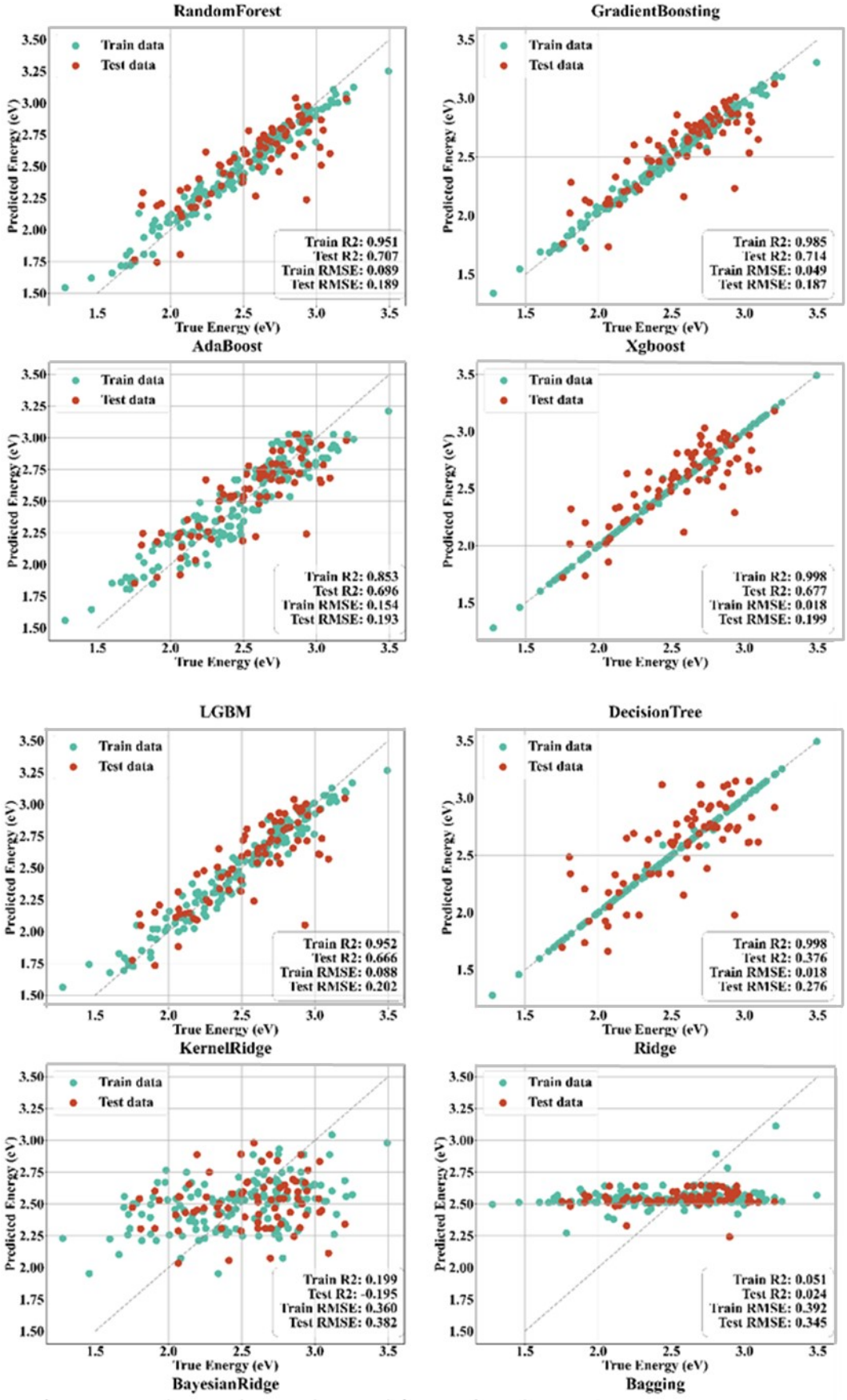

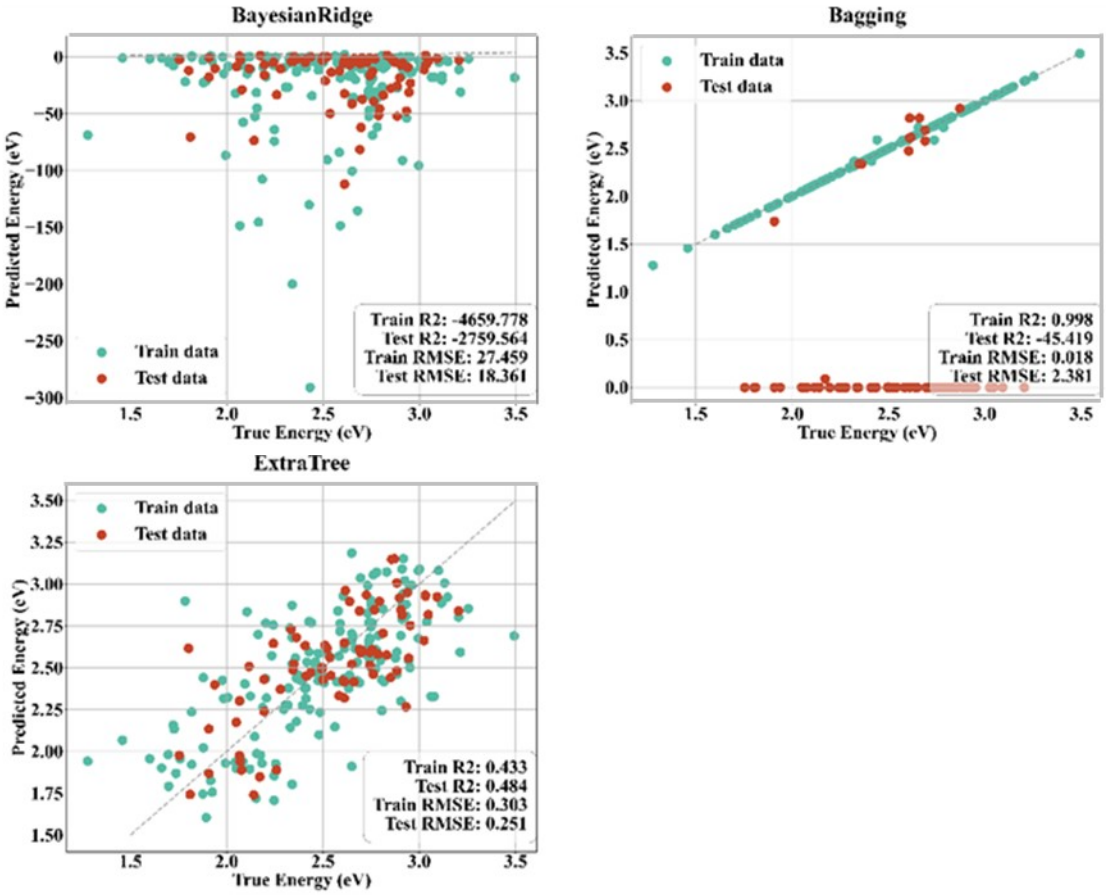

Figure S14 The fitting performance of eleven models on the training and testing sets of ASE wavelength data

Evaluation and Optimization of Models

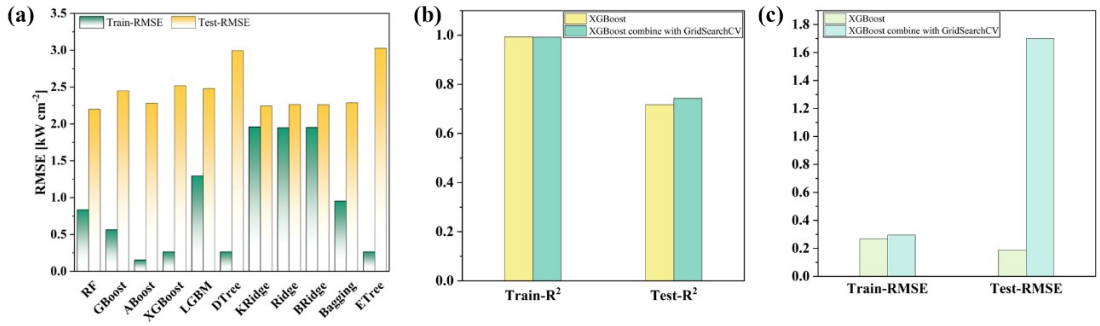

Figure S15 The ASE threshold (a)The RMSE of the eleven ASE threshold models;(b) The R^2 comparison of the best model, XGBoost, before and after hyperparameter optimization using GridSearchCV; (c) The RMSE comparison of the best model, XGBoost, before and after hyperparameter optimization using GridSearchCV.

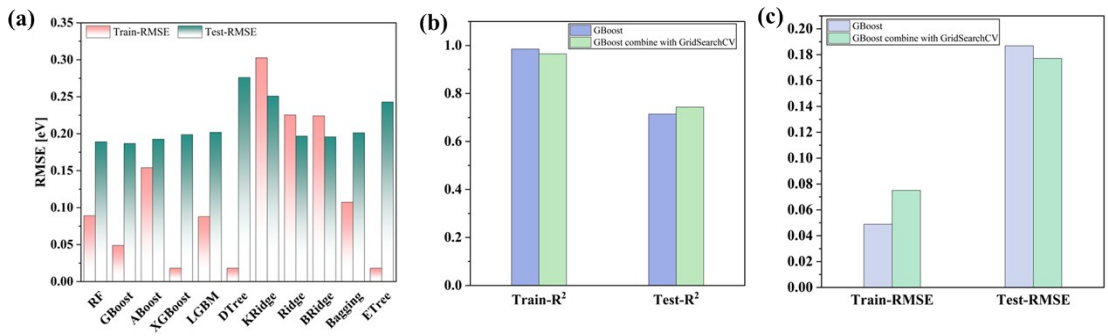

Figure S16 The ASE wavelength (a)The RMSE of the eleven ASE wavelength models;(b) The R^2 comparison of the best model, GBoost, before and after hyperparameter optimization using GridSearchCV; (c) The RMSE comparison of the best model, GBoost, before and after hyperparameter optimization using GridSearchCV.

Feature Importance Chart and SHAP Chart

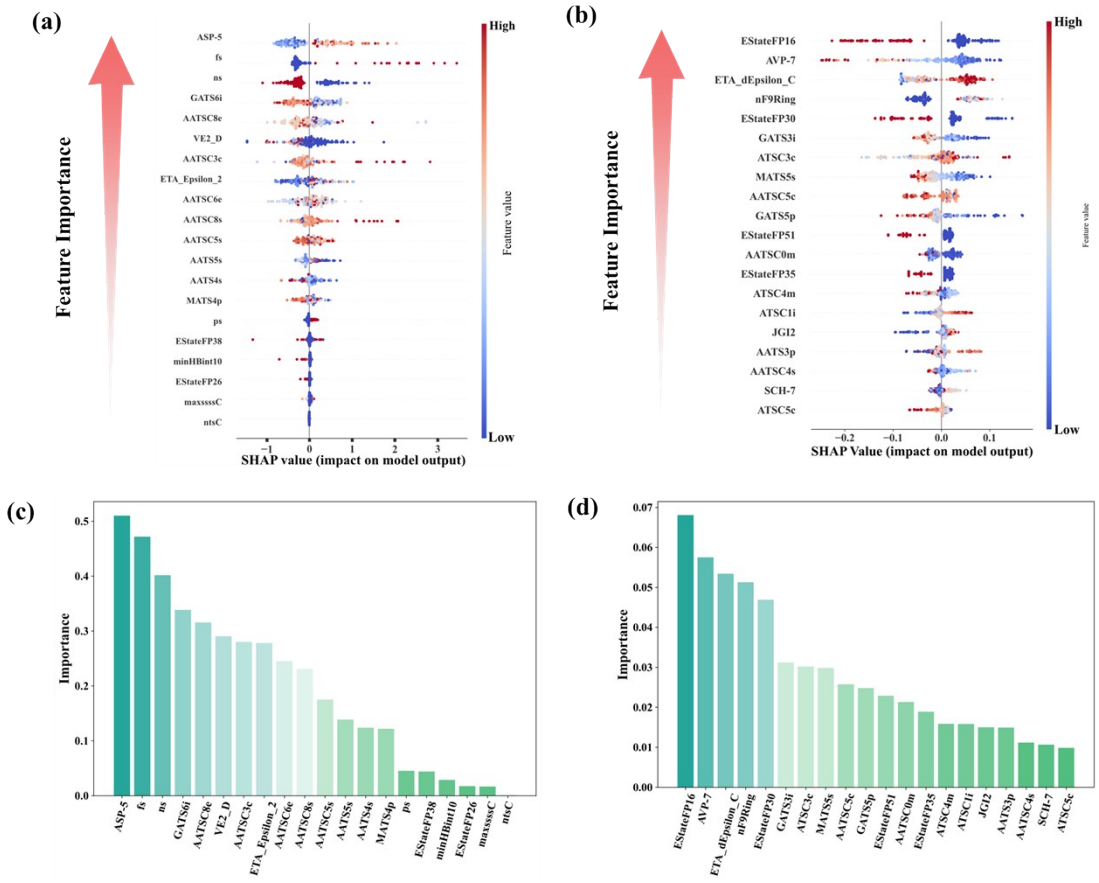

Figure S17 The SHAP analysis prediction of ML mixed regression model is ranked based on the significance of diverse characteristics (a, b) The driving or hindering impacts on ASE threshold and wavelength are displayed in the SHAP value table. Each dot represents the SHAP value for a feature across the dataset, with the color indicating the actual value of the features. Features are ranked by the impact on the output of the model, with positive SHAP values driving higher ASE threshold and wavelength predictions and negative values indicating a reduction in ASE threshold and ASE wavelength. (c, b) The bar chart provides a more intuitive visualization of the feature importance rankings for the ASE threshold and wavelength model.

Figure S17a shows the SHAP plots for the ASE threshold from the Xgboost model, while Figure S17c highlights the feature contributions. The top ten most important feature descriptors for the ASE threshold model include autocorrelation descriptors (GATS6i, AATSC8e, AATSC3c, GATS5i, AATSC6e and AATSC8s), time scale

descriptors (fs, ns), weighted distance matrix descriptors (VE2_D), topochemical descriptors (ASP-5), and extended topochemical atom descriptors (ETA_Epsilon_2) (Table S3). Notably, the top three features (≥ 0.5 for APS-5 and ≥ 0.4 for fs and ns) account for over 50% of the importance in the ASE threshold model. ASP-5 and fs show a positive correlation with the ASE threshold, while ns exhibits a negative correlation with it. The ASE threshold is closely related to the optical gain and excited-state behavior of the material. ASP-5 influences the processes of light absorption, emission, and electron transfer by revealing the topological structure of specific atoms and their neighboring atoms within the molecule. A higher ASP-5 value indicates that certain atoms occupy significant positions in the molecular topological structure, enabling effective energy transfer, which in turn affects the energy loss in excited states and alters the ASE threshold.

Similarly, the top ten most important features for the ASE wavelength rank as the EStateFP16 ([CD3H0](=*)(-*)-*), AVP-7 (Average valence path, order 7), ETA_dEpsilon_C(A measure of electronegative atom count), nF9Ring (Number of 9-membered fused rings), EstateFP30 ([ND3H0](-*)(-*)-*), GATS3i (Geary autocorrelation—lag 3/weighted by first ionization potential), ATSC3c(Centered Broto-Moreau autocorrelation-lag 3/weighted by charges), MATS5s (Moran autocorrelation—lag 5/weighted by I-state), AATSC5p (centered Broto-Moreau autocorrelation—lag 5/weighted by polarizability) and GATS5p (Geary autocorrelation—lag 5/weighted by polarizability) (Table S4). Notably, the importance of the top four features (nearly 0.07 for EStateFP16 and more than 0.05 for AVP-7, ETA_dEpsilon_C and nF9Ring) contributed more than 50% of importance for the ASE wavelength, as shown in Figure S17b, d. The structure where a carbon atom is connected by both a single bond and a double bond is found to be negatively correlated with the ASE wavelength. This is because the structure enhances the molecular conjugation effect, reduces the electronic transition energy gap, and consequently causes a redshift in the ASE wavelength.

Model prediction

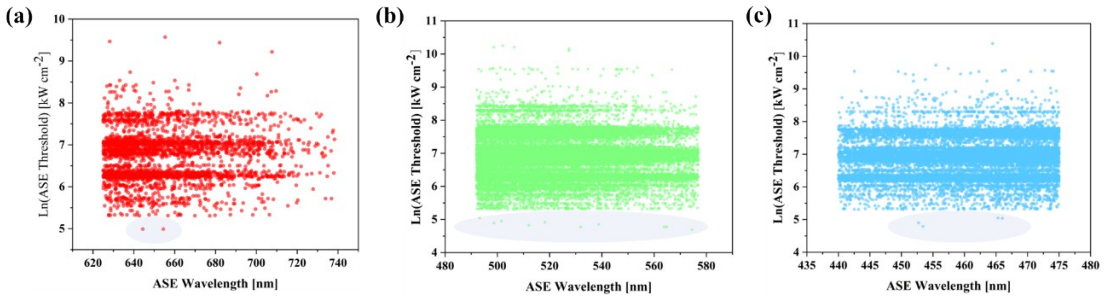

Figure S18 The distribution of predicted ASE wavelength and ASE threshold for organic laser molecules in the (a)red, (b)green, and (c)blue regions.

Below are the molecular structures corresponding to the circled areas in the figure above:

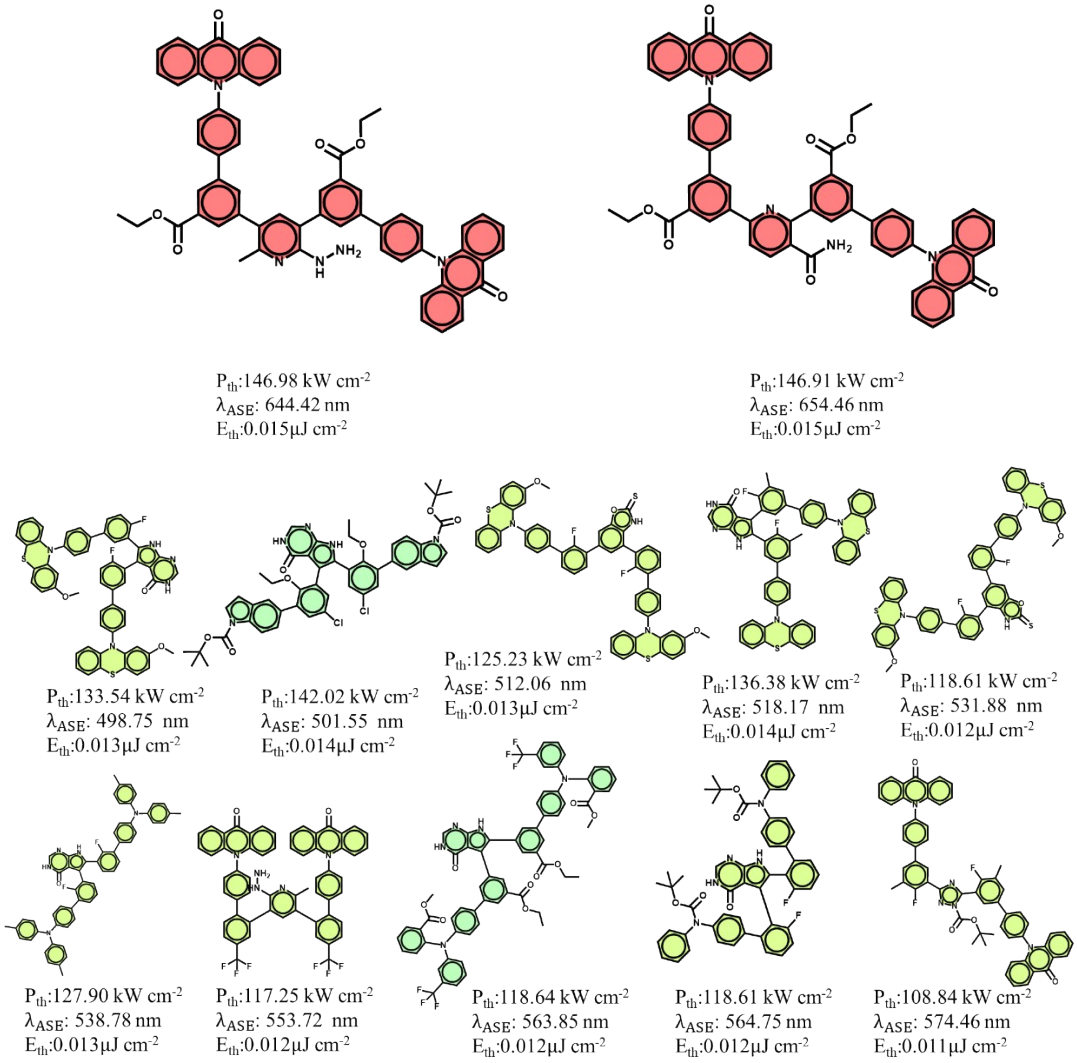

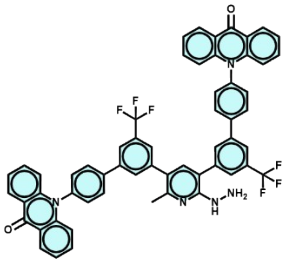

P_{th}:118.61 kW cm^{-2}
λ_{ASE}: 454.72 nm
E_{th}:0.012μJ cm^{-2}

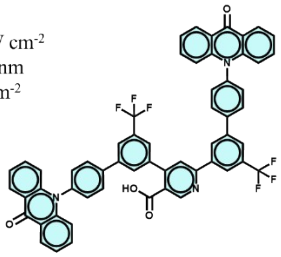

P_{th}:114.34 kW cm^{-2}
λ_{ASE}: 456.58 nm
E_{th}:0.011μJ cm^{-2}

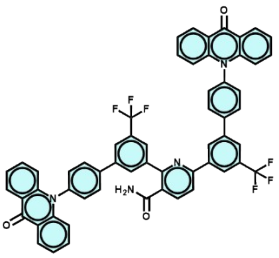

P_{th}:117.25 kW cm^{-2}
λ_{ASE}: 461.17 nm
E_{th}:0.012μJ cm^{-2}

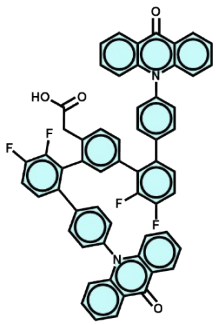

P_{th}:119.00 kW cm^{-2}
λ_{ASE}: 450.25 nm
E_{th}:0.012μJ cm^{-2}

Comparison of predicted results with previous results

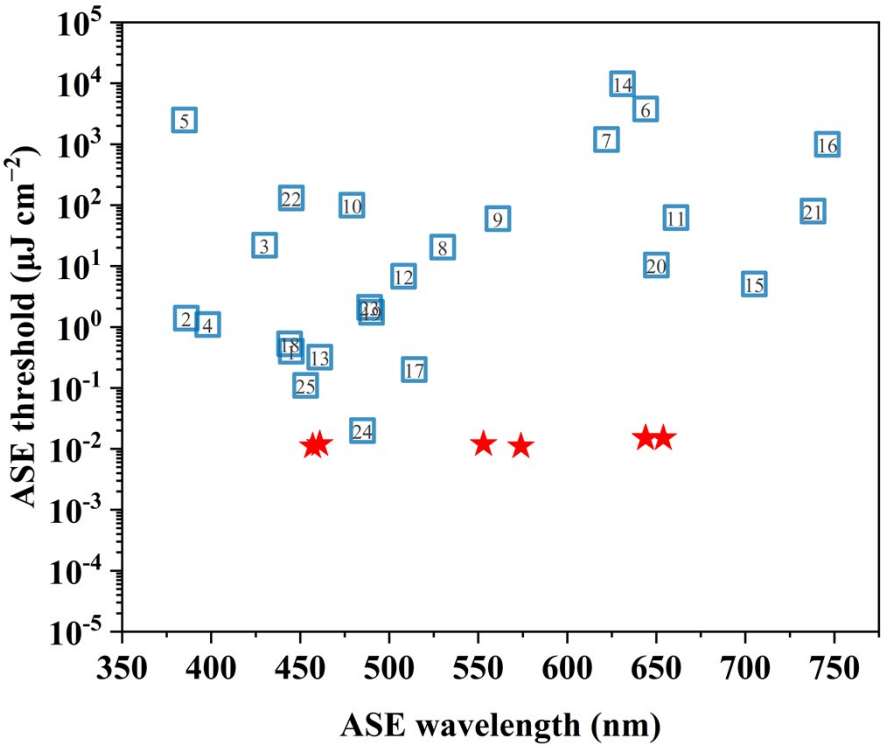

Figure S19 Comparison of machine learning predictions with representative experimental results from the past 30 years.

Synthetic Route for Candidate Molecules

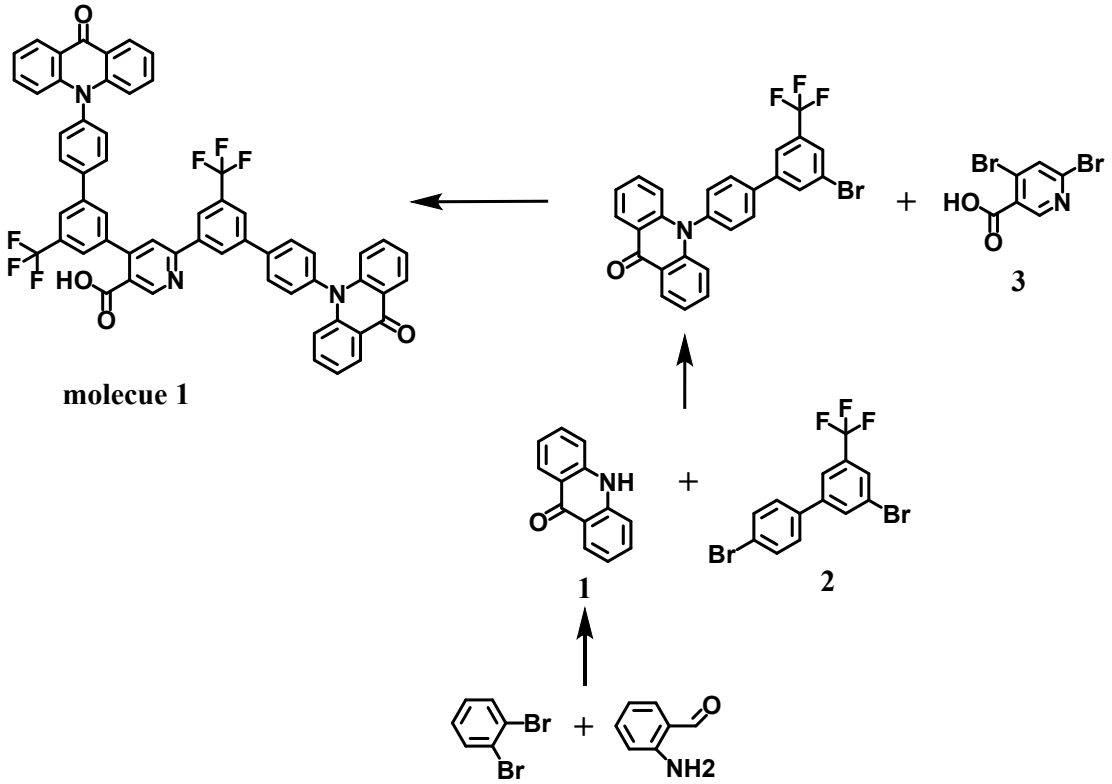

Figure S20 Synthesis of molecule 1.

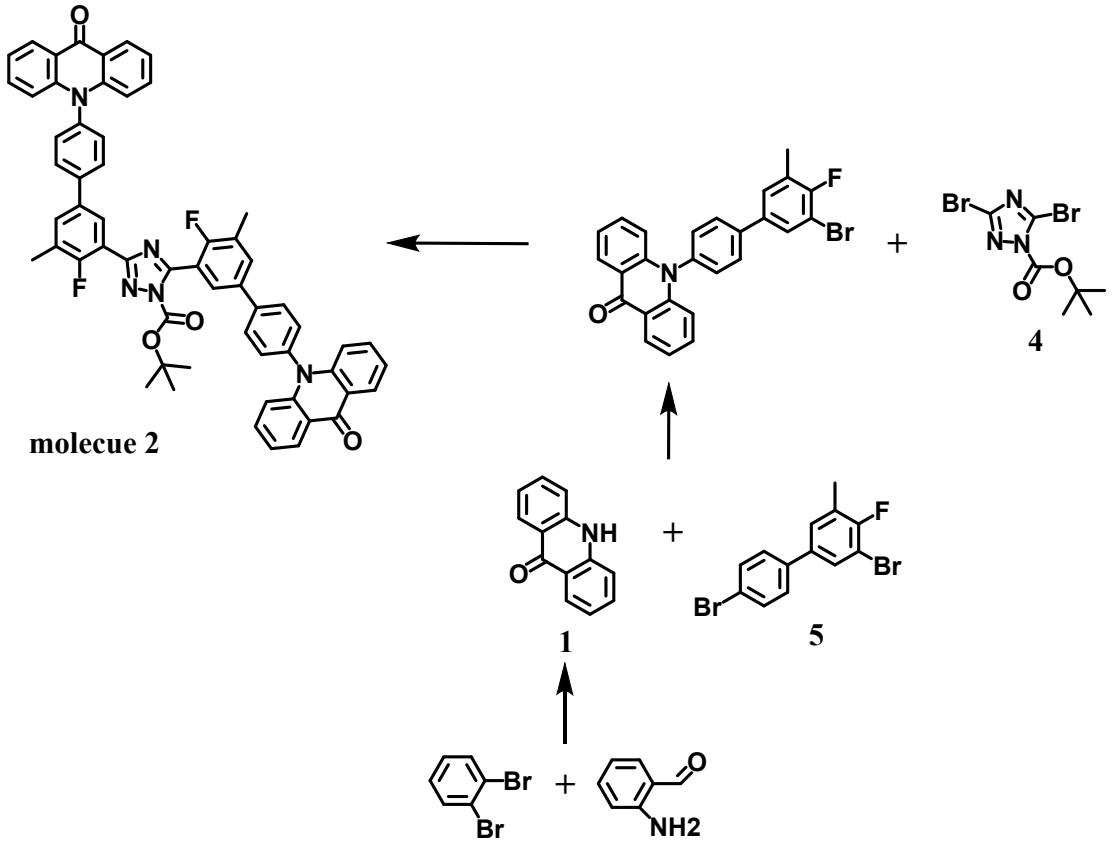

Figure S21 Synthesis of molecule 2.

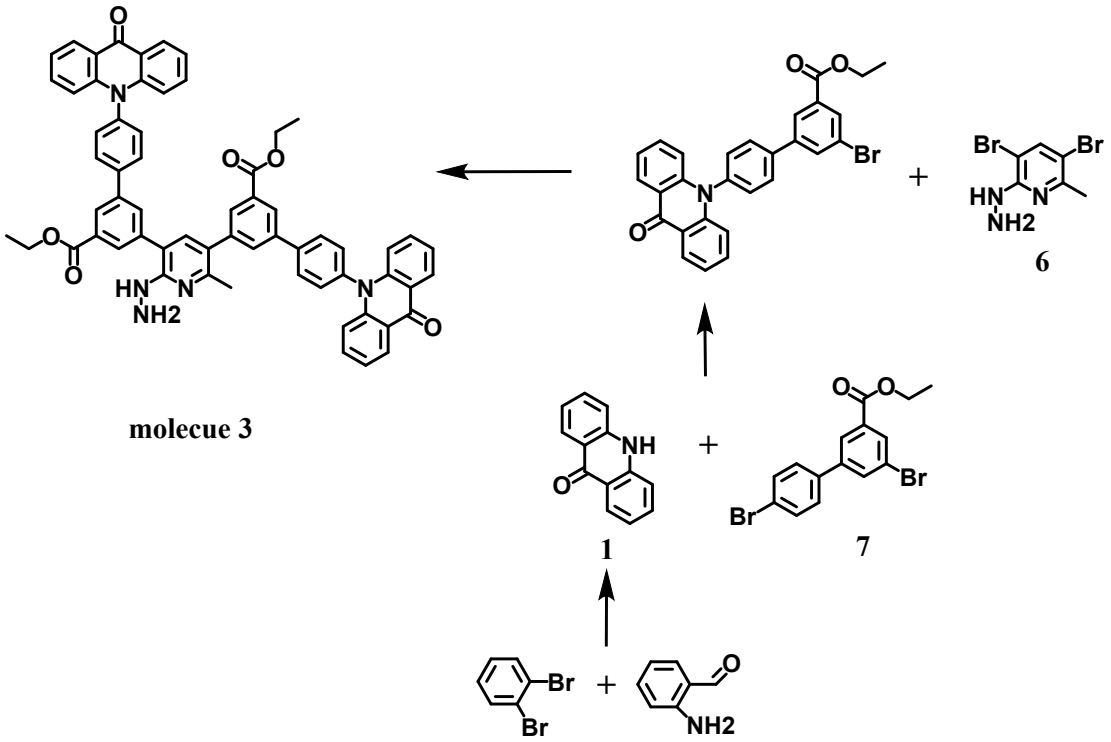

Figure S22 Synthesis of molecule 3.

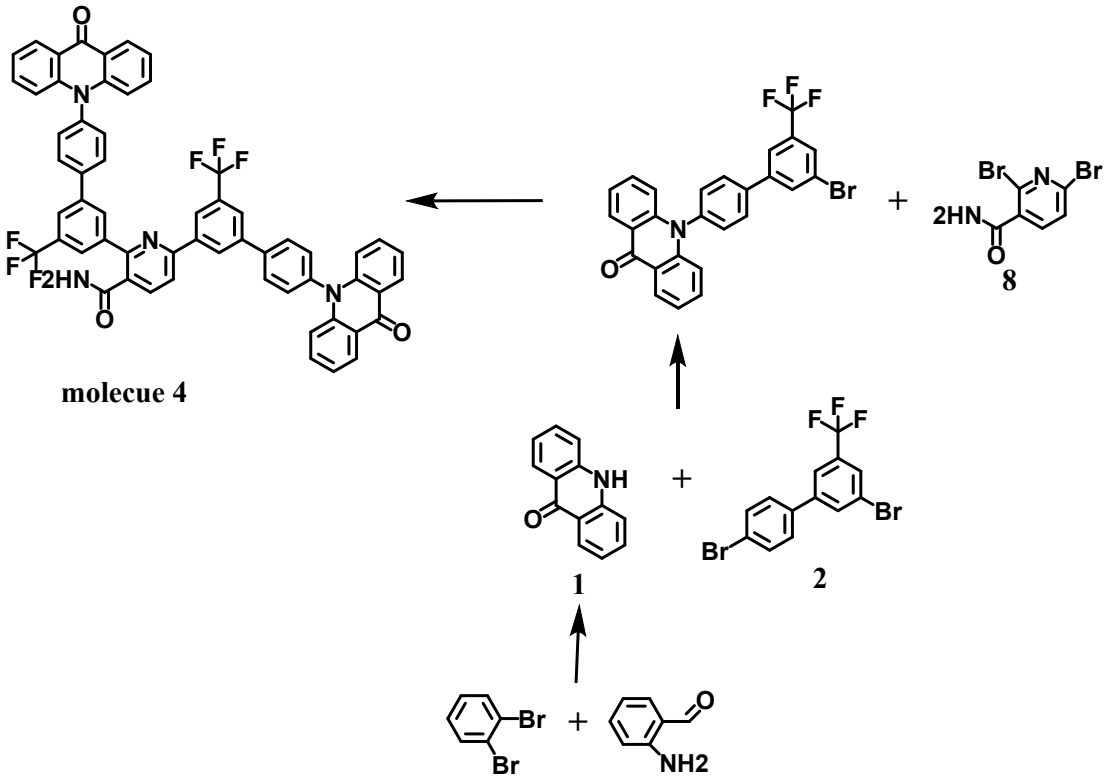

Figure S23 Synthesis of molecule 4.

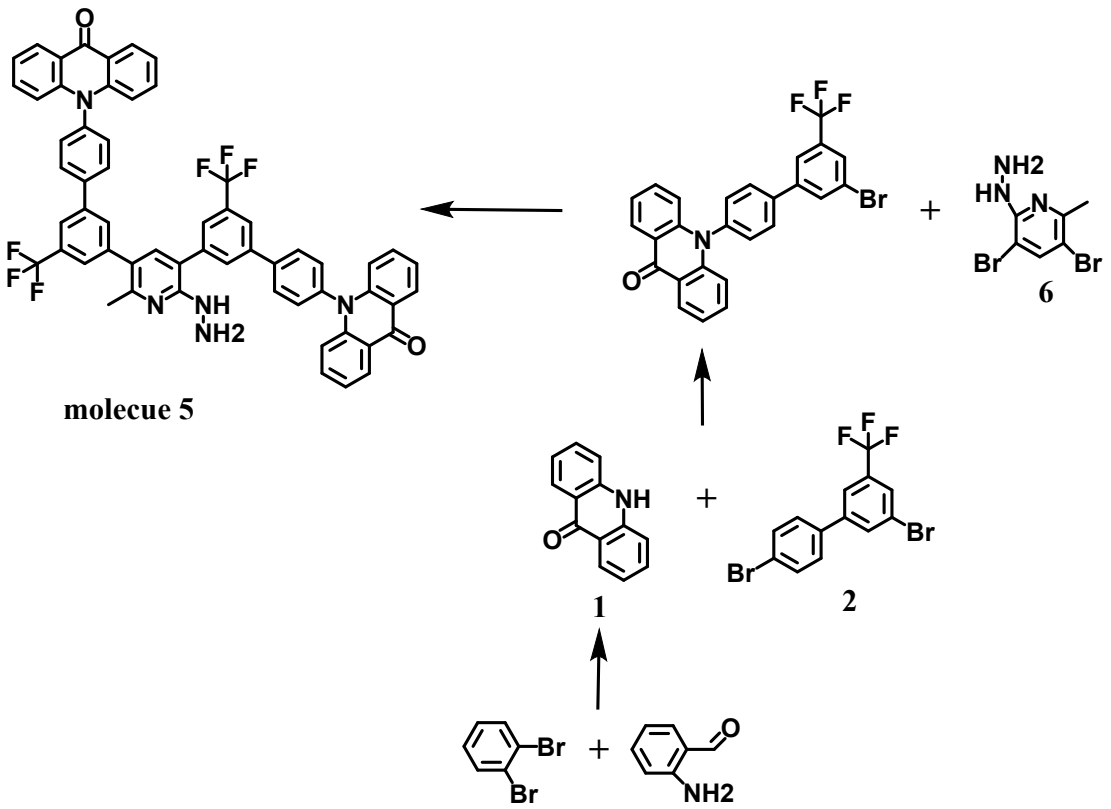

Figure S24 Synthesis of molecule 5.

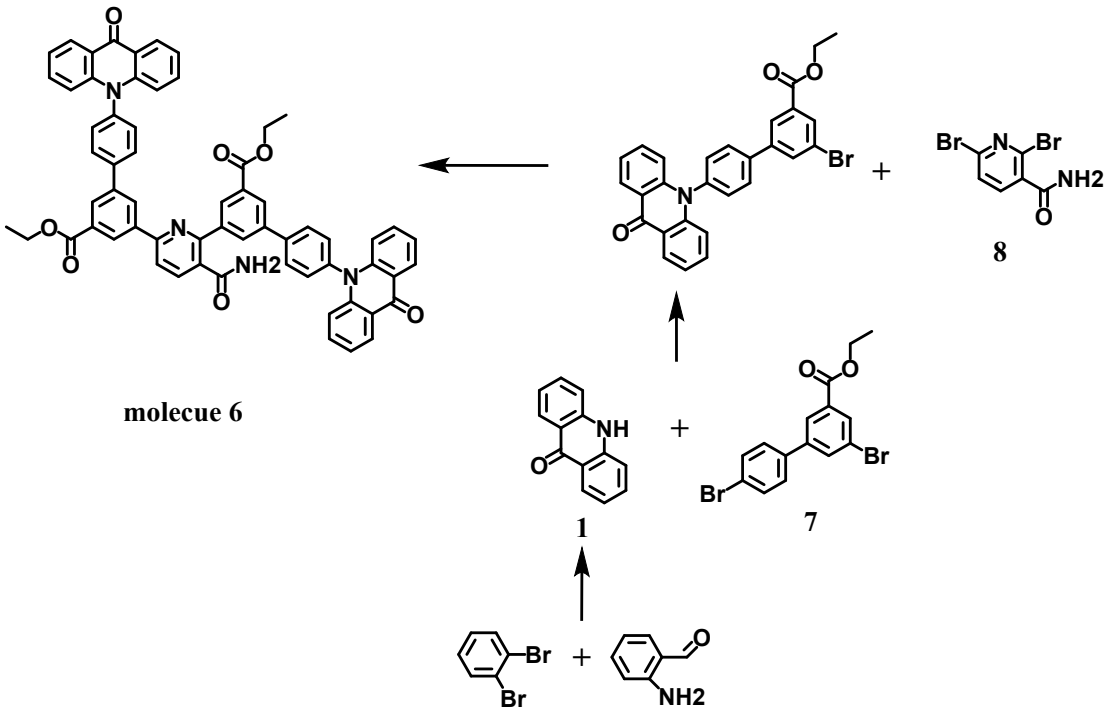

Figure S25 Synthesis of molecule 6.

Monomer 1 can be synthesized by reacting biphenyl dibromide with 2-amino-benzaldehyde, both of which can be directly purchased. Monomers 3, 4, and 8 are also readily available. For Monomer 2, there is a structurally similar compound, 1,1′-Biphenyl, 2,4′-dibromo-5-(trifluoromethyl)- (ACI). Due to the strong electron-withdrawing effect of the trifluoromethyl group, it usually causes the bromine atom to be positioned in the para position relative to the trifluoromethyl group, making electrophilic substitution reactions more likely to occur at the para position. This is because the para product is more stable and symmetrical, making it more suitable for practical applications. In contrast, the meta product is less stable, harder to separate, and less in demand, making it less likely to form in chemical reactions. Monomer 5 has a similar structure, such as 1,1′-Biphenyl, 3-bromo-4-fluoro-5-methyl- (ACI) and 1,1′-Biphenyl, 3-bromo-4,4′-difluoro-5-methyl- (ACI). The coexistence of bromine and fluorine may cause internal instability within the molecule, particularly in terms of the selectivity of the reaction site on the benzene ring. The electron-withdrawing effects of fluorine and bromine may lead to uneven electron density distribution on the aromatic ring, affecting the molecule's stability. Monomer 6 has structural analogs such as 2-Pyridinamine, 3,5-dibromo-N,6-dimethyl-(9CI, ACI) and 2-Pyridinamine, 3,5-dibromo-6-methyl-(9CI, ACI). The amino group is an electron-donating group, which increases the electron density on the benzene ring, facilitating addition reactions. Monomer 7 has a similar structure to 1,1′-Biphenyl-3-carboxylic acid, 4′-bromo-, ethyl ester (ACI). The bromine atom, being an electron-withdrawing group, typically exerts an inductive electron-withdrawing effect that can extend up to the third carbon, causing structural instability.

Code abstract

```
from sklearn.preprocessing import StandardScaler
from sklearn.feature_selection import RFE
from sklearn.model_selection import cross_val_score, GridSearchCV
from sklearn import metrics
from sklearn import datasets
from sklearn.linear_model import LinearRegression
from sklearn.tree import DecisionTreeRegressor
from sklearn.ensemble import GradientBoostingRegressor
from sklearn.neural_network import MLPRegressor
from sklearn.ensemble import AdaBoostRegressor
from sklearn.ensemble import ExtraTreesRegressor
from sklearn.ensemble import RandomForestRegressor
from sklearn.svm import LinearSVR
from sklearn.svm import NuSVR
from sklearn.svm import SVR
from xgboost import XGBRegressor
from sklearn.metrics import accuracy_score
import numpy as np
import pandas as pd
import shap
import matplotlib.pyplot as plt
from sklearn.model_selection import train_test_split
df = pd.read_csv()
features = df.iloc[:,1:].values
target= df.iloc[:,0].values
X_train, X_test, y_train, y_test
=train_test_split(features,target,test_size=0.2,random_state=0)
model=randomforest.fit(X_train, y_train)
y_pred = randomforest.predict(X_test)
```

```
yt = randomforest.predict(X_train)
importances = list(model.feature_importances_)
feature_name = list(df.columns)[1:]
feature_importances = [(feature, round(importance, 2))
for feature, importance in zip(feature_name, importances)]
feature_importances = sorted(feature_importances, key = lambda x: x[1], reverse =
True)
estimator_list =[RandomForestRegressor(),
GradientBoostingRegressor(),
LinearRegression(),
DecisionTreeRegressor(),
MLPRegressor(solver='lbfgs'),
AdaBoostRegressor(),
ExtraTreesRegressor(),
LinearSVR(),
SVR(),
XGBRegressor(nthread = 15) ]
cv_split = ShuffleSplit(n_splits=3,test_size=0.3, random_state=0)
df_columns = ['Name', 'Parameters', 'Train Accuracy Mean', 'Test Accuracy Mean',
'TestAccuracyStd','ComsumedTime']
df = pd.DataFrame(columns=df_columns)

RFE
X=data.iloc[:,1:]
y=data.iloc[:,0]
estimator = LinearRegression()
n_features_to_select = 20
selector = RFE(estimator, n_features_to_select=n_features_to_select)
X_selected = selector.fit_transform(X, y)
selected_features = selector.support_
```

```
print(f"Number of selected features: {X_selected.shape[1]}")
print("Ranking of selected features:")
print(selector.ranking_)
```

PLOT:

```
fontsize=12
plt.figure(figsize=(3.5,3))
plt.style.use('default')
plt.rc('xtick', labelsize=fontsize)
plt.rc('ytick', labelsize=fontsize)
plt.rcParams['font.family']="Arial"
a = plt.scatter(y_train, yt, s=25,c='LightSkyBlue')
b = plt.scatter(y_test, y_pred, s=25,c='PaleGreen')
plt.tick_params(direction='in')
plt.legend((a,b),('Train','Test'),fontsize=fontsize,handletextpad=0.1,borderpad=0.1)
plt.rcParams['font.family']="Arial"
plt.plot([0.5,1.7],[0.5,1.7],"--",color="black")
plt.tight_layout()
```

SHAP:

```
model.fit(X_test,y_test)
explainer = shap.TreeExplainer(model)
shap_values = explainer.shap_values(X_test)
shap_explainer = explainer(X_test)
shap_explainer.base_values=shap_explainer.base_values[0][0]
shap_explainer.data=shap_explainer.data[]
shap_explainer.values=shap_explainer.values[]
shap.initjs()
shap.summary_plot(shap_values.values,X_test,show = False,alpha = 0.6,max_display
= 15)
```

Table S1 Performance evaluation metrics of the ASE threshold models

Model	R^2 (Train)	RMSE on train set	R^2 on test set	RMSE on test set
Random Forest	0.889	1.071	0.585	2.131
Gradient Boosting	0.973	0.531	0.515	2.298
Adaboost	0.824	1.350	0.529	2.265
Xgboost	0.993	0.268	0.717	1.756
LightGBM	0.796	1.453	0.593	2.106
Decision Tree	0.993	0.269	0.153	3.049
Kernel Ridge	0.429	2.433	0.541	2.237
Ridge	0.432	2.426	0.589	2.116
Bayesian Ridge	0.408	2.478	0.566	2.175
Bagging	0.857	1.217	0.513	2.301
Extra Tree	0.993	0.233	0.269	2.895

Table S2 Performance evaluation metrics of the ASE wavelength models

Machine-learning techniques	R^2 on train set	RMSE on train set	R^2 on test set	RMSE on test set
Random Forest	0.951	0.089	0.707	0.189
Gradient Boosting	0.985	0.049	0.714	0.187
Adaboost	0.853	0.154	0.696	0.193
Xgboost	0.998	0.018	0.677	0.199
LightGBM	0.952	0.088	0.666	0.202
Decision Tree	0.998	0.018	0.375	0.276
Kernel Ridge	0.433	0.0303	0.484	0.251
Ridge	0.686	0.226	0.683	0.197
Bayesian Ridge	0.689	0.224	0.686	0.196
Bagging	0.929	0.107	0.668	0.201
Extra Tree	0.998	0.018	0.517	0.243

Table S3 Selected 20 descriptors based on feature importance analysis and correlation analysis for the ASE threshold of organic laser molecules

Name	Description
ns	The pulse time scale of the pump source is nanosecond level
ps	The pulse time scale of the pump source is picosecond
fs	The pulse time scale of the pump source is in the order of seconds
AATSC3c	centered Broto-Moreau autocorrelation—lag 3/weighted by charges
AATSC6e	centered Broto-Moreau autocorrelation—lag 6/weighted by Sanderson electronegativity
AATSC8e	centered Broto-Moreau autocorrelation—lag 8/weighted by Sanderson electronegativity
AATSC8s	centered Broto-Moreau autocorrelation—lag 8/weighted by intrinsic state
MATS4p	Moran autocorrelation—lag 4/weighted by polarizability
GATS6i	Geary autocorrelation—lag 6/weighted by first ionization potential
ASP-5	Average simple path, order 5
ETA_Epsilon_2	A measure of electronegative atom count
VE2_D	Average coefficient sum of the last eigenvector from Barysz matrix/weighted by atomic number
EStateFP26	tN, [ND1H0]#*
EStateFP38	sF, [FD1]-*
maxssssC	Maximum atom-type E-State: >C<
AATS4s	Lag 4/weighted by intrinsic state for the centering of the Broto-Moreau autocorrelation
AATS5s	Lag 5/weighted by intrinsic state for the centering of the Broto-Moreau autocorrelation
AATSC5s	centered Broto-Moreau autocorrelation—lag 5/weighted by intrinsic state
ntsC	Count of atom-type E-State: #C-
minHBint10	minimum E-state descriptors of strength for potential hydrogen bonds of path length 10

Table S4 Selected 20 descriptors based on feature importance analysis and correlation analysis for the ASE wavelength of organic laser molecules

Name	Description
EstateFP16	[CD3H0](=*)(-*)-* , dssC
EstateFP30	[ND3H0](-*)(-*)-* , aaN
EstateFP35	[OD1H0]=* , sOH
EstateFP51	[S,sD2H0](:*):* , aaS
AATS3p	ATS autocorrelation descriptor, weighted by polarizability
ATSC3c	Centered Broto-Moreau autocorrelation-lag 3/weighted by charges
ATSC5c	Centered Broto-Moreau autocorrelation-lag 5/weighted by charges
ATSC4m	ATS autocorrelation descriptor, weighted by scaled atomic mass
ATSC1i	ATS autocorrelation descriptor, weighted by charges
AATSC5c	Average Atom Type Specific Charge 5 Connectivity
AATSC0m	Average Atom Type Specific Charge 0 Connectivity
AATSC4s	Average Atom Type Specific Charge 4 Shortest Path Connectivity
MATS5s	Moran autocorrelation—lag 5/weighted by I-state
GATS5p	Geary autocorrelation—lag 5/weighted by polarizability
GATS3i	Geary autocorrelation—lag 5/weighted by I-state
SCH-7	Simple chain, order 7
AVP-7	Average valence path, order 7
ETA_dEpsilon_C	captures details about how electronic properties or energies change within the molecular structure. This can include information about how electronic distributions or interactions influence the overall molecular characteristics.
nF9Ring	Number of 9-membered fused rings
JGI2	Junction Geometry Index 2

References

1. E. Y. Choi , L. Mazur , L. Mager , M. Gwon , D. Pitrat , J. C. Mulatier , C. Monnereau , A. Fort , A. J. Attias , K. Dorkenoo , J. E. Kwon , Y. Xiao , K. Matczyszyn , M. Samoc , D. W. Kim , A. Nakao , B. Heinrich , D. Hashizume , M. Uchiyama , S. Y. Park , F. Mathevet , T. Aoyama , C. Andraud , J. W. Wu , A. Barsella and J. C. Ribierre , Phys. Chem. Chem. Phys., 2014, 16 , 16941 —16956

2. J.-C. Ribierre , L. Zhao , M. Inoue , P.-O. Schwartz , J.-H. Kim , K. Yoshida , A. S. D. Sandanayaka , H. Nakanotani , L. Mager , S. Mery and C. Adachi , Chem. Commun., 2016, 52 , 3103 —3106

3. K. Kazlauskas , G. Kreiza , O. Bobrovas , O. Adomeniene , P. Adomenas , V. Jankauskas and S. Jursenas , Appl. Phys. Lett., 2015, 107 , 043301

4. T. Oyamada , C. H. Chang , T. C. Chao , F. C. Fang , C. C. Wu , K. T. Wong , H. Sasabe and C. Adachi , J. Phys. Chem. C, 2007, 111 , 108 —115

5. M. Morales-Vidal , P. G. Boj , J. M. Villalvilla , J. A. Quintana , Q. Yan , N.-T. Lin , X. Zhu , N. Ruangsupapichat , J. Casado , H. Tsuji , E. Nakamura and M. A. Diaz-Garcia , Nat. Commun., 2015, 6 , 8458

6. J. Huang , Q. Liu , J. H. Zou , X. H. Zhu , A. Y. Li , J. W. Li , S. Wu , J. Peng , Y. Cao , R. Xia , D. D. C. Bradley and J. Roncali , Adv. Funct. Mater., 2009, 19 , 2978 —2986

7. M. G. Ramirez , S. Pla , P. G. Boj , J. M. Villalvilla , J. A. Quintana , M. A. Diaz-Garcia , F. Fernandez-Lazaro and A. Sastre-Santos , Adv. Opt. Mater., 2013, 1 , 933 —938

8. M. Sang , S. Cao , J. Yi , J. Huang , W.-Y. Lai and W. Huang , RSC Adv., 2016, 6 , 6266 —6275

9. C. R. Belton , A. L. Kanibolotsky , J. Kirkpatrick , C. Orofino , S. E. T. Elmasly , P. N. Stavrinou , P. J. Skabara and D. D. C. Bradley , Adv. Funct. Mater., 2013, 23 , 2792 —2804

10. F. Laquai , A. K. Mishra , K. Muellen and R. H. Friend , Adv. Funct. Mater., 2008, 18 , 3265 —3275

11. R. Xia , P. N. Stavrinou , D. D. C. Bradley and Y. Kim , J. Appl. Phys., 2012, 111 , 123107

12. M. Sang , S. Cao , J. Yi , J. Huang , W.-Y. Lai and W. Huang , RSC Adv., 2016, 6 , 6266 —

6275

13. A. S. D. Sandanayaka , T. Matsushima , F. Bencheikh , K. Yoshida , M. Inoue , T. Fujihara , K. Goushi , J.-C. Ribierre and C. Adachi , Sci. Adv., 2017, 3 , e1602570

14. L. Wang , Z. Zhang , X. Cheng , K. Ye , F. Li , Y. Wang and H. Zhang , J. Mater. Chem. C, 2015, 3 , 499 —505

15. X. Wang , Q. Liao , H. Li , S. Bai , Y. Wu , X. Lu , H. Hu , Q. Shi and H. Fu , J. Am. Chem. Soc., 2015, 137 , 9289 —9295

16. C. Xiao , W. Kai , H. Shuo , Z. Houyu , Z. Hongyu and W. Yue , Angew. Chem., Int. Ed., 2015, 54 , 8369 —8373

17. W. Zhang , Y. Yan , J. Gu , J. Yao and Y. S. Zhao , Angew. Chem., Int. Ed., 2015, 54 , 7125 —7129

18. Q. Wei , Y. Li , J. Liu , Q. Fang , J. Li , X. Yan , L. Xie , Y. Qian , R. Xia and W. Huang , Adv. Opt. Mater., 2017, 5 , 1601003

19. R. Xia , W.-Y. Lai , P. A. Levermore , W. Huang and D. D. C. Bradley , Adv. Funct. Mater., 2009, 19 , 2844 —2850

20. Z. Yu , Y. Wu , L. Xiao , J. Chen , Q. Liao , J. Yao and H. Fu , J. Am. Chem. Soc., 2017, 139 , 6376 —6381

21. H. Ye , D. H. Kim , X. Chen , A. S. D. Sandanayaka , J. U. Kim , E. Zaborova , G. Canard , Y. Tsuchiya , E. Y. Choi , J. W. Wu , F. Fages , J.-L. Bredas , A. D'Aléo , J.-C. Ribierre and C. Adachi , Chem. Mater., 2018, 30 , 6702 —6710

22. R. D. Xia , G. Heliotis , Y. B. Hou and D. D. C. Bradley , Org. Electron., 2003, 4 , 165 —177

23. M. Fang , J. Huang , Y. Zhang , X. Guo , X. Zhang , C. F. Liu , W.-Y. Lai and W. Huang , Mater. Chem. Front., 2017, 1 , 668 —676

24. Tae-Woo Lee, O Ok Park, Dong Hoon Choi, Hyun Nam Cho, Young Chul Kim; Appl. Phys. Lett. 15 July 2002; 81 (3): 424–426.

25. Nakanotani, H., Akiyama, S., Ohnishi, D., Moriwake, M., Yahiro, M., Yoshihara, T., Tobita, S. and Adachi, C. (2007), Adv. Funct. Mater., 17: 2328-2335.